Real-Time Observation of Discrete Andreev Tunneling Events

V. F. Maisi,[1,2,*] O.-P. Saira,[1] Yu. A. Pashkin,[3,†] J. S. Tsai,[3] D. V. Averin,[4] and J. P. Pekola[1]

[1]*Low Temperature Laboratory, Aalto University, P.O. Box 13500, 00076 Aalto, Finland*
[2]*Centre for Metrology and Accreditation (MIKES), P.O. Box 9, 02151 Espoo, Finland*
[3]*NEC Green Innovation Research Laboratories and RIKEN Advanced Science Institute,*
34 Miyukigaoka, Tsukuba, Ibaraki 305-8501, Japan
[4]*Department of Physics and Astronomy, Stony Brook University, SUNY, Stony Brook, New York 11794-3800, USA*
(Received 28 February 2011; published 25 May 2011)

We provide a direct proof of two-electron Andreev transitions in a superconductor–normal-metal tunnel junction by detecting them in a real-time electron counting experiment. Our results are consistent with ballistic Andreev transport with an order of magnitude higher rate than expected for a uniform barrier, suggesting that only part of the interface is effectively contributing to the transport. These findings are quantitatively supported by our direct current measurements in single-electron transistors with similar tunnel barriers.

Electronic transport across a boundary between conductors with dissimilar carriers is a nontrivial process. Of particular interest in this respect is the transport through a superconductor–normal-metal interface that at low energies is dominated by Andreev reflection [1–10], where a Cooper pair in a superconductor is converted into two electrons in the normal metal or vice versa. Here we employ electron counting techniques [11–17] to detect these Andreev events. Since the observed rate depends on the coherence of the two electrons involved in the transition, we obtain, as a result, a fingerprint of the junction electrodes and the tunnel barrier.

The techniques used for observing individual electrons are based on the Coulomb blockade effect where the electrostatic energy of a small metallic island changes noticeably when only one elementary charge e is placed on or removed from it. In the present experiment, we employ an isolated single-electron box where a superconducting island is connected to a normal metal one [17], but neither of these two is connected galvanically to the external circuitry. The electron tunneling rates between the islands are then sufficiently low to be monitored by low-frequency electrometry and are described in detail by relatively simple theoretical considerations [17,18]. We use a single-electron transistor (SET) [11–15,17,19–22] as an ultrasensitive electrometer. With charge sensitivity as good as $10^{-5}e/\sqrt{\text{Hz}}$ [22–24], it is capable to detect individual electrons with high precision. In Fig. 1, we show a micrograph of our sample fabricated by standard e-beam processing.

The tunneling rates and resulting charge distribution between the two islands of the isolated box can be adjusted with an offset charge induced by a gate voltage. The electrostatic energy of a state with n excess electrons on one of the islands is given by $E_n = E_c(n - n_g)^2$, where E_c is the charging energy for individual electrons and n_g is the

normalized offset charge that can be viewed as the polarization charge on the gate capacitor and determines the energetically preferred way to occupy the different charge states n [20]. In Fig. 2(a), the two extreme cases are shown. In the Coulomb blockade regime for single electrons, n_g is an integer and the state $n = n_g$ has the minimal energy $E_n = 0$. To enter an excited state, one electron can tunnel either into or out of the island [dotted black lines with arrows in Fig. 2(a)], but energy E_c has to be provided for the tunneling electron in addition to the Cooper pair breaking energy equal to or larger than the superconducting energy gap Δ [25]. In the other extreme, at degeneracy with half-integer n_g, two electron states differing by charge e have equal minimal energy and hence are equally populated. The tunneling rate between them is higher than in the Coulomb blockade regime as no extra energy for charging is needed. For Andreev reflection [solid red lines with
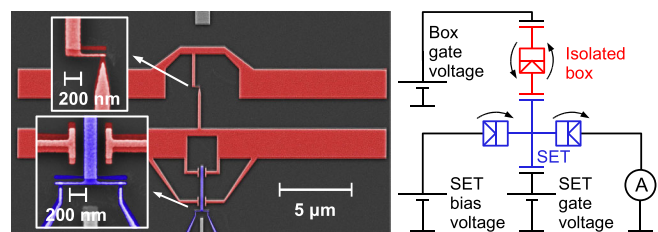

FIG. 1 (color online). Scanning electron micrograph of the measured structure and the schematic layout of the measurement setup. The isolated electron box consists of two metallic islands, seen as 25 μm long rectangles (colored red). They are connected to each other by a normal-metal–insulator–superconductor tunnel junction. Tunneling of electrons through the junction is monitored with a dc SET electrometer (in blue) coupled capacitively to one of the box islands. The normal-metal–insulator–superconductor junction (top) and detector (bottom) are shown magnified on the left side of the main micrograph.
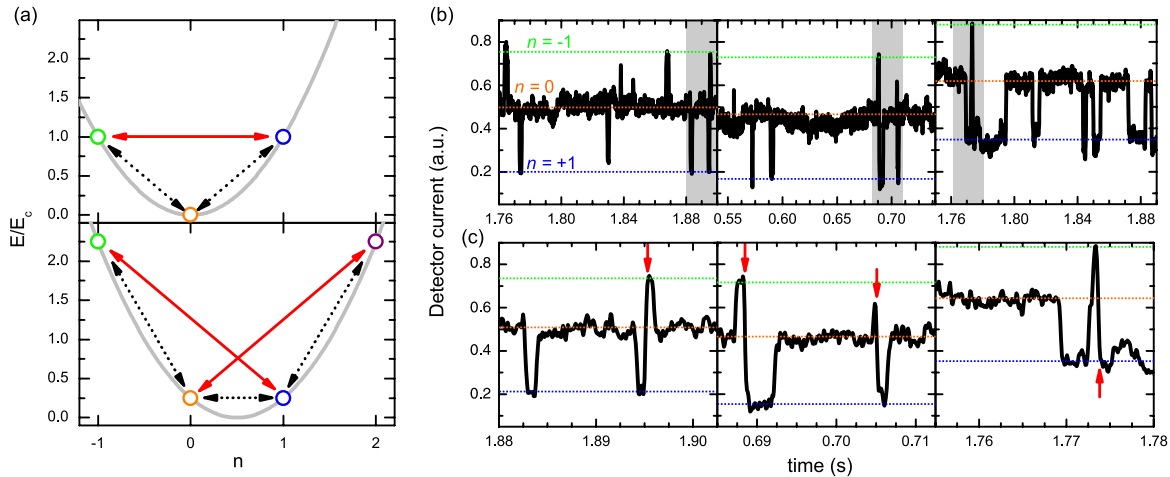
FIG. 2 (color online).   Energy levels of the various charge states and typical observed time traces of the current through the detector.
(a) Low lying levels of the box in the Coulomb blockade (upper panel) and at degeneracy (lower panel). Dotted (black) and solid (red)
arrows indicate one- and two-electron processes, respectively. (b) Measured time traces of the detector current showing the charge state
of the electron box as a function of time. The leftmost panel presents the case of Coulomb blockade. The rightmost panel depicts the
opposite limit where the two charge states are equal in energy (degeneracy). The trace in the center is taken halfway between these two
cases. (c) Gray sections of the traces of (b) zoomed. Vertical arrows indicate two-electron events.

arrows in Fig. 2(a)], the energy cost of charging is
calculated similarly, but now the initial and final states
are separated by two electrons, and the energy cost of
breaking a Cooper pair is avoided since complete pairs
tunnel at once.

  In the experiment (see the supplemental material for
additional details [26]), we measured time traces of the
detector current at various biasing conditions of the box.
With all the other parameters fixed, the detector gate
voltage was adjusted to maximize charge sensitivity and
dynamic range. The observed current jumps [Figs. 2(b) and
2(c)] are attributed to the tunneling events between the two
islands. The switching rate depends on the gate voltage of
the box and hence on its charge state, being lowest in the
Coulomb blockade regime (leftmost panel) and highest at
degeneracy (rightmost panel). The events observed in the
traces [gray regions of Fig. 2(b) zoomed in 2(c)] indicate
that individual electrons tunnel between the islands: In the
Coulomb blockade regime they hop rarely from the lowest
($n = 0$) to the higher ($n = \pm 1$) energy states and back,
while at degeneracy the electrons tunnel frequently be-
tween the two lowest states and only occasionally the
system enters a higher lying level. More interestingly,
the traces also show the coincident events, pointed out by
the vertical arrows, where two electrons appear to tunnel
simultaneously. In the following, we show that most of
these events represent Andreev tunneling.

  Because of the finite measurement bandwidth, limited to
1 kHz by the dc readout of the electrometer, events resem-
bling two-electron Andreev tunneling could in principle
arise from almost coincidental tunneling of two indepen-
dent quasiparticles. To assess this option, we recorded time
traces for several minutes at each gate offset value.
From the traces we determined the distribution of the

time t spent in the state $n = 0$ before a transition took
place. In Fig. 3(a), we show such a distribution on the left
for Coulomb blockade ($n_g = 0$), in the center for $n_g = 0.25$,
and on the right for near degeneracy ($n_g = 0.45$). A direct
transition (Andreev tunneling) between states $n = \pm 1$
contributes here as essentially a $t = 0$ event since the
time separation between the two electrons tunneling in
the Andreev process should be on the order of $\hbar/\Delta$, which
is many orders of magnitude smaller than the time scales
relevant in Fig. 3(a). Overall, the distribution is exponential
as we have Poisson distributed one-electron tunneling
processes. However, at small lifetimes in the Coulomb
blockade regime, the data point indicated by the horizontal
arrow does not follow the exponential dependence and
corresponds to excessively many events. This clear sepa-
ration of the short-lifetime events from the one-electron
transitions shows that the majority of these events are not
coincidental one-electron tunneling but rather two elec-
trons tunneling concurrently. When the box offset charge is
adjusted closer to degeneracy, the anomalous data point
gradually merges to the rest of the data, in accordance with
its interpretation in terms of Andreev transitions, since the
energy cost of the two-electron tunneling increases.
We emphasize that the charging energy should be small
($E_c < \Delta$) for Andreev tunneling to occur, since for large
E_c, it is not energetically favorable [17].

  For quantitative analysis, we counted the number of
events N_j for each possible forward and backward one-
and two-electron tunneling process for each initial charge
state n. The corresponding tunneling rate was then ob-
tained as $\Gamma_j = N_j/(\langle t \rangle N_\Sigma)$, where $\langle t \rangle$ is the average life-
time of the initial state n and N_Σ the total number of all
transitions out of this state. The denominator $\langle t \rangle N_\Sigma$ there-
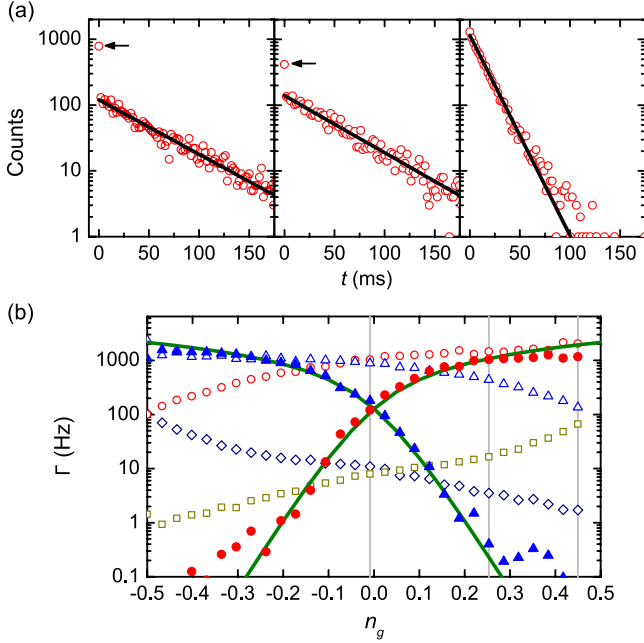fore corresponds to the total time spent in the initial state.

FIG. 3 (color online). Lifetime distributions and tunneling rates. (a) Lifetime distributions of the $n = 0$ charge state in the Coulomb blockade, at an intermediate gate position, and close to degeneracy, from left to right. The corresponding gate positions are indicated by vertical lines in (b). Excessively many events at small times are pointed out by horizontal arrows. (b) One-electron (open symbols) and two-electron (solid symbols) tunneling rates estimated from the counted events at the base temperature. Red circles and blue triangles denote the tunneling rates out of states $n = -1$ and 1, respectively. Dark blue diamonds and dark yellow squares denote tunneling rates out of state 0 to states -1 and 1, respectively. Dark green solid lines present calculated Andreev rates with $\zeta = 4 \times 10^{-5}$.

Transitions with the charge number changing by $\Delta n = \pm 2$ and occurring within 0.4 ms were interpreted as two-electron tunneling and all other events as one-electron tunneling. The time window was chosen such that it essentially captures all the excess events shown in the histograms of Fig. 3(a) but minimizes the number of coincidental one-electron events. The results for both processes at the temperature of 60 mK are shown in Fig. 3(b). The parameter values which determine the first-order tunneling rates in the box junction, the tunneling resistance $R_T = 2$ MΩ, the superconducting energy gap $\Delta = 216$ μeV, and the charging energy $E_c = 0.2\Delta$, were determined from the one-electron tunneling rates measured at temperatures ranging from 60 to 200 mK as in Ref. [17].

For analyzing the Andreev tunneling rates quantitatively, we assume a ballistic model of the tunnel barrier. Then, the rate is given by Eq. (3) of Ref. [27]. Apart from the parameter values obtained from one-electron tunneling, the only parameter to be determined for the two-electron tunneling is its overall magnitude controlled by $\zeta \equiv (\hbar/R_T e^2)/\mathcal{N}$, where $\mathcal{N}$ is the effective number of the conduction channels in the junction, $\mathcal{N} = A/A_{ch}$. Here A_{ch} is the area of one conduction channel and

$A = 40$ nm $\times 35$ nm the junction area estimated from the scanning electron micrograph. Ideally, for our aluminum oxide tunnel barriers one should have $A_{ch} \simeq 2$ nm²; see the supplemental material [26]. However, to fit the observed tunneling rates, we must adopt an order of magnitude higher value, $A_{ch} = 30$ nm², leading to an order of magnitude higher rates. As a result, we obtain the green lines of Fig. 3(b) for forward and backward tunneling, demonstrating a good agreement between theory and experiments at different charging energy costs tuned by n_g.

An order of magnitude larger area of a conduction channel is in line with independently performed SET measurements described in detail below and with the conclusions in, e.g., Refs. [6,10], for larger tunnel junctions that exhibit diffusive Andreev tunneling. We attribute this to the imperfections of the barrier, with only a small portion of the junction area dominating the transport. This fact can be understood by noting that the standard parameters of the aluminum oxide tunnel barriers [26,28,29] imply that, for example, variation of the barrier thickness by one atomic layer (i.e., by about 0.3 nm) results in the specific conductance change by about a factor of 10. This means that even relatively small fluctuations of the barrier thickness of the magnitude of one to two atomic layers in comparison with the average barrier thickness of 6 atomic layers can reduce the effective area of the region dominating the barrier transparency to about 10% of the total junction area.

As an additional way of studying the two-electron tunneling, we measured current-voltage characteristics of basic SET structures with superconducting leads and a normal metal island. A micrograph of one of the four devices is shown in the inset in Fig. 4. All the SETs were fabricated in the same batch so that the junction area (E_c) varies with constant $\zeta \propto (A R_T)^{-1}$. Here Andreev tunneling has to be extracted from the measured data containing a contribution also from one-electron processes. Each of the SETs was biased at voltage V, and the current I flowing through the device was measured. At each bias voltage, the gate offset of the island was varied so that the maximal and minimal currents, corresponding to degeneracy and Coulomb blockade, respectively, were observed. The measured current values between these extremes are shown as the colored regions in Fig. 4 for the four devices having different E_c. The parameter values for E_c, R_T, and Δ were determined from large scale data dominated by one-electron tunneling. Insets show the data for samples with the highest and lowest E_c. In the subgap region $eV < 2\Delta$, we have no current flowing through the highest charging energy sample (top) apart from the thermally activated single-electron tunneling. With smaller E_c, the onset of the Andreev current penetrates deeper into the subgap region with the threshold at $eV = 2E_c$, seen both in the experimental data and in the fits including Andreev processes (solid black lines), as the energy cost for two electrons tunneling into the island is lowered. With high
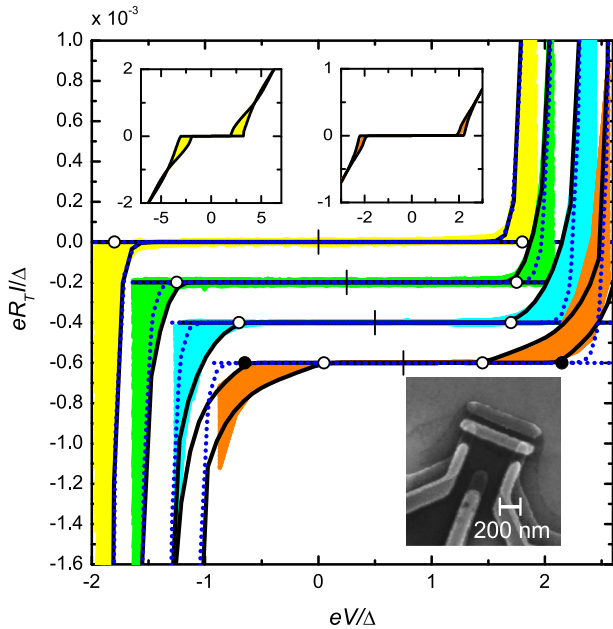
FIG. 4 (color online). Detection of Andreev current in SETs. Colored regions show measured subgap current for devices with charging energies $E_c/k_B = 2.3$, 1.9, 1.5, and 0.86 K from top (yellow) to bottom (orange) at all gate offset values. The insets depict the larger scale measurements for samples with the highest and lowest charging energies and a scanning electron micrograph of one of the measured SETs. Solid black lines are fitted theoretical curves at degeneracy (maximal current) and in Coulomb blockade (minimal current) when Andreev tunneling is taken into account. Dotted blue lines present fits excluding Andreev processes. Tunneling resistances of the samples were $R_T = 129$, 78, 55, and 31 kΩ in order of decreasing E_c, and superconducting gap $\Delta = 216$ μeV for all of them. Open (solid) circles present the expected thresholds $eV = \pm 2E_c$ ($eV = \pm 4E_c$) for Andreev tunneling at degeneracy (Coulomb blockade).

charging energies $E_c \gtrsim \Delta$, it is sufficient to take into account only one-electron tunneling in the fits (dotted blue lines). In the numerical simulations for all the samples, we obtain as the only fit parameter for the subgap currents $\zeta \approx 4 \times 10^{-4}$, yielding the area of one conduction channel to be $A_{ch} = 30$ nm^2. This value was adopted to the analysis of the counting data above. Note that to increase the measured signal the SET junctions were oxidized less to have larger specific conductance (ζ) than the box junction.

In conclusion, we have detected tunneling in the time domain, allowing us to distinguish two-electron Andreev transitions from the usual one-electron processes unambiguously and on the level of individual events. This technique, unlike the direct current measurements, addresses the transition rates in the two directions separately, allowing for the study of the bias dependence of these rates also in the regime where currents are far too low to be detected by standard current measurements. The counting experiments disclose the detailed statistics of the two

processes, and the results are consistent with the direct current measurements performed: As a technological result, both measurements indicate that the tunnel barriers are nonuniform.

*ville.maisi@mikes.fi
†On leave from Lebedev Physical Institute, Moscow 119991, Russia.

[1] A. F. Andreev, Zh. Eksp. Teor. Fiz. **46**, 1823 (1964) [Sov. Phys. JETP **19**, 1228 (1964)].
[2] G. E. Blonder, M. Tinkham, and T. M. Klapwijk, Phys. Rev. B **25**, 4515 (1982).
[3] T. M. Eiles, J. M. Martinis, and M. H. Devoret, Phys. Rev. Lett. **70**, 1862 (1993).
[4] P. Lafarge et al., Nature (London) **365**, 422 (1993).
[5] F. W. J. Hekking and Y. V. Nazarov, Phys. Rev. B **49**, 6847 (1994).
[6] H. Pothier et al., Phys. Rev. Lett. **73**, 2488 (1994).
[7] S. Rajauria et al., Phys. Rev. Lett. **100**, 207002 (2008).
[8] A. S. Vasenko et al., Phys. Rev. B **81**, 094513 (2010).
[9] J. Wei and V. Chandrasekhar, Nature Phys. **6**, 494 (2010).
[10] T. Greibe et al., Phys. Rev. Lett. **106**, 097001 (2011).
[11] J. M. Martinis, M. Nahum, and H. D. Jensen, Phys. Rev. Lett. **72**, 904 (1994).
[12] P. D. Dresselhaus et al., Phys. Rev. Lett. **72**, 3226 (1994).
[13] S. V. Lotkhov et al., Appl. Phys. Lett. **75**, 2665 (1999).
[14] W. Lu et al., Nature (London) **423**, 422 (2003).
[15] J. Bylander, T. Duty, and P. Delsing, Nature (London) **434**, 361 (2005).
[16] T. Fujisawa et al., Science **312**, 1634 (2006).
[17] O.-P. Saira et al., Phys. Rev. B **82**, 155443 (2010).
[18] J. P. Pekola et al., Phys. Rev. Lett. **105**, 026803 (2010).
[19] P. Lafarge et al., Z. Phys. B **85**, 327 (1991).
[20] D. V. Averin and K. K. Likharev, J. Low Temp. Phys. **62**, 345 (1986).
[21] T. A. Fulton and G. J. Dolan, Phys. Rev. Lett. **59**, 109 (1987).
[22] G. Zimmerli et al., Appl. Phys. Lett. **61**, 237 (1992).
[23] V. A. Krupenin et al., J. Appl. Phys. **84**, 3212 (1998).
[24] L. Roschier et al., Appl. Phys. Lett. **78**, 3295 (2001).
[25] I. Giaever, Phys. Rev. Lett. **5**, 147 (1960).
[26] See supplemental material at http://link.aps.org/supplemental/10.1103/PhysRevLett.106.217003 for details about sample fabrication, measurements, data analysis, and channel size estimate.
[27] D. V. Averin and J. P. Pekola, Phys. Rev. Lett. **101**, 066801 (2008).
[28] Z. Tan et al., Appl. Phys. Lett. **93**, 242109 (2008).
[29] M. Prunnila et al., J. Vac. Sci. Technol. B **28**, 1026 (2010).